

A quantum mechanical study of bioactive 3-chloro-2,5-dihydroxybenzyl alcohol through substitutions

Anoja Pushpamali Wickrama Arachchilage ·
Yong Wang · Feng Wang

Received: 5 May 2011 / Accepted: 3 September 2011 / Published online: 1 October 2011
© Springer-Verlag 2011

Abstract Electronic structures, vibrational and ionization spectra of 3-chloro-2,5-dihydroxybenzyl alcohol (CHBA), a novel bioactive benzene derivative from marine fungi, are presented in this study using quantum mechanical methods such as density functional theory and outer valence Green function method. A number of related benzene derivatives such as chlorobenzene, 3-chlorobenzyl alcohol, hydroquinone and chlorohydroquinone are also studied, in order to assist our understanding of the structure, properties and interactions of CHBA. Vibrational spectra such as infrared (IR) and Raman spectra reveal signatures of the functional group substitutions and their hydrogen bond interactions in CHBA. Solvent effects on the IR spectra of CHBA with polar and non-polar solvents are simulated using the polarizable continuum model (PCM) and cause redshifts of some of the IR spectral frequencies with respect to the gas phase values at both ends of the 400–4,000 cm^{-1} region. The inner-shell ionization spectra, in particular the C–K spectra of the benzene derivatives, reveal detailed chemical environmental changes of the carbon and oxygen atoms due to the substitutions. The valence ionization energies of the highest occupied molecular orbital (HOMO) and the 3rd HOMO, (HOMO-2) of the benzene derivatives respond significantly to the substitutions, whereas the charge

distributions of the HOMO and 2nd HOMO (HOMO-1) do not change significantly from their benzene counterparts. As a result, the 3rd HOMO changes significantly in both ionization energies and the charge distributions, which can serve as a signature of the substitutions among the benzene derivatives.

Keywords Density functional theory study · Bioactive compounds · 3-chloro-2,5-dihydroxybenzyl alcohol · Benzene derivatives · Electronic structures · IR and Raman spectroscopy and ionization spectroscopy

1 Introduction

Natural products have provided the inspiration for most of the active ingredients in medicines and have been the most productive source of leads for new drugs [1]. The exploration of the bioactivity of natural products continues to provide novel chemical scaffolds for further drug inventions [2, 3]. There is an increasing need for the development and analysis of novel biologically active natural products. This is due to the emergence of resistant strains of pathogens, the appearance of new diseases, and the inadequacy or toxicity of current drugs [4]. In the search for novel and bioactive molecules for drug discovery, the source is largely from three major groups: the plant kingdom, the microbial world, and the marine world. In the last 30 years, there has been an explosive growth of natural products from the marine world that has been characterized by the isolation and structure elucidation of very diverse structures with no precedent in terrestrial natural products [1]. For example, natural products from marine prokaryotes that are available in marine environments provide a tremendous opportunity for the discovery of novel therapeutic

Dedicated to Professor Akira Imamura on the occasion of his 77th birthday and published as part of the Imamura Festschrift Issue.

A. P. W. Arachchilage · F. Wang (✉)
Faculty of Life and Social Sciences, Swinburne University
of Technology, Hawthorn, Melbourne, VIC 3122, Australia
e-mail: fwang@swin.edu.au

Y. Wang
Chongqing Institute for Drug Control, Chongqing 401121,
People's Republic of China

agents. Furthermore, the primary chemical diversity available from marine prokaryotes is most likely capable of delivering an even greater abundance of natural products.

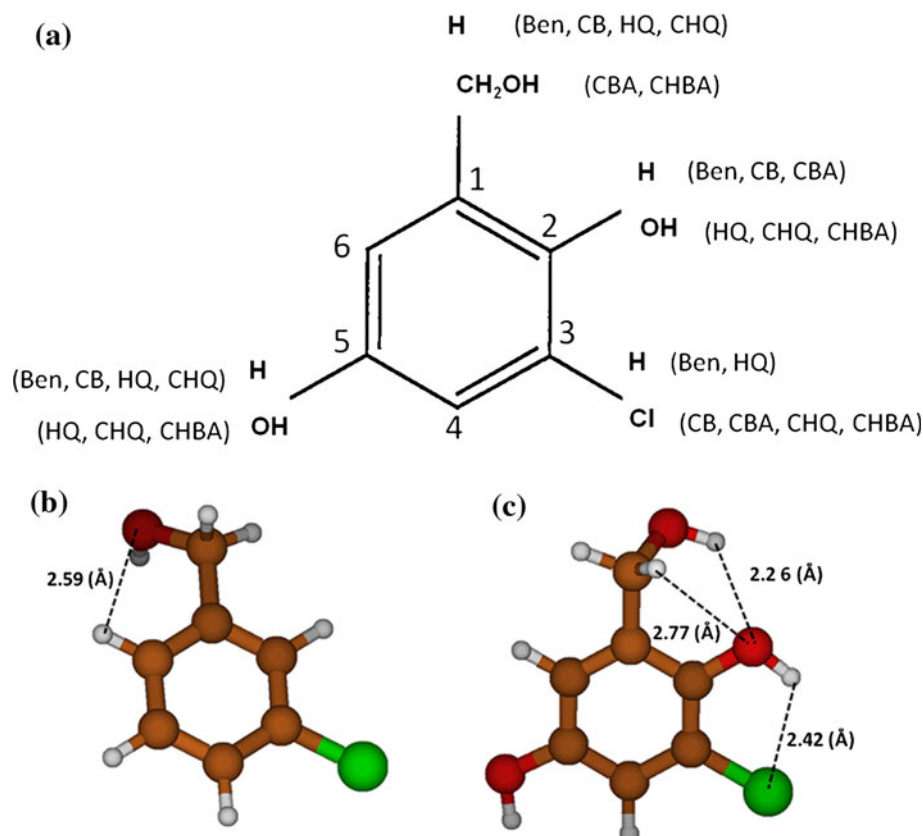
A bioactive antifouling and antimicrobial compound, 3-chloro-2,5-dihydroxybenzyl alcohol ($C_7H_7O_3Cl$, namely, CHBA), a benzene derivative, was recently isolated from a marine-derived fungus *Ampelomyces* sp. from sea water near Hong Kong [5]. It was first isolated from fungus *Phoma* sp. in 1971 by Sequin-Frey and Tamm [6], and later it was isolated from *Penicillium canadense* [7], *Phyllosticta* sp. [8], *Aspergillus* sp. [9] and more recently from marine [5] and terrestrial [10] *Ampelomyces* sp. In the earlier days, little information about the properties of the compound was known, except for its phytotoxic browning effect on red clove leaves [8]. The antifouling and antimicrobial activities of CHBA suggest it as a substitution for currently using antifouling paints, which show high toxicity to the marine fauna and flora [5, 10]. Furthermore, the ability of 3-chloro-2,5-dihydroxybenzyl alcohol to induce apoptosis in human cervical carcinoma HeLa cells [9] suggests the potential applications of CHBA as an anticancer drug candidate.

Due to the pharmaceutical applications of CHBA as an anticancer drug candidate, a clear understanding of the function of the compound is required, which requires the study of its structure [11]. The chemical composition of

CHBA was identified as $C_7H_7O_3Cl$ by McCorkindale et al. [7] using UV and NMR techniques. A more recent isolation has identified further the benzene derivative structure as shown in Fig. 1, that is, three major functional groups such as hydroxymethyl, hydroxyl and chlorine substitute the hydrogen atoms on the unsubstituted benzene. Benzene and substituted benzene derivatives are excellent candidates to study the Hoffmann-Imamura-Hehre (HIH) through-space (TS)–through-bond (TB) interactions [12] in order to better understand the functional group and their impact on the structure and properties of CHBA. The present study employs quantum mechanical approaches such as density functional theory (DFT) and outer valence Green function (OVGF) combined with functional group substitution studies to explore the electronic structural impact on the unsubstituted benzene. In this study, the functional groups, i.e., hydroxymethyl ($-CH_2OH$), hydroxyl ($-OH$) and chlorine (Cl), are substituted for the hydrogen atoms of benzene to form benzene derivatives, in order to reveal the ultimate structure and properties, as well as the TS and TB interactions of the functional groups of the 3-chloro-2,5-dihydroxybenzyl alcohol compound.

Figure 1 gives the substitution scheme of the benzene derivatives. The unsubstituted benzene (C_6H_6) serves as a reference for the benzene derivatives in the study. As shown in Fig. 1, from a chemical point of view, 3-chloro-

Fig. 1 a Schematic diagram of 3-chloro-2,5-dihydroxybenzyl alcohol (CHBA) and model benzene derivative molecules, chlorobenzene (CB), 3-chlorobenzyl alcohol (CBA), hydroquinone (HQ) and chlorohydroquinone (CHQ). The optimized three-dimensional structures of CBA (b) and CHBA (c) are given in b and c, respectively, with important O...H distances



2,5-dihydroxybenzyl alcohol (CHBA) is a benzene derivative in which chlorine (Cl) replaces the hydrogen atom at the C(3) position, one hydroxymethyl ($-\text{CH}_2\text{OH}$) group replaces the hydrogen atom at the C(1) position and two hydroxyl ($-\text{OH}$) groups replace the hydrogen atoms at the C(2) and C(5) positions, respectively. One produces chlorobenzene ($\text{C}_6\text{H}_5\text{Cl}$, CB) when the hydrogen atom at C(3) of benzene is replaced by Cl (single substitution); 3-chlorobenzyl alcohol (CBA) is produced when the hydrogen atom of CB is replaced by hydroxymethyl at the C(1) position; hydroquinone (HQ) is produced when the hydrogen atoms at the C(2) and C(5) positions are replaced by the $-\text{OH}$ groups (double substitutions); and chlorohydroquinone (CHQ) is produced when the hydrogen atom at the C(3) position of HQ is replaced by Cl (triple substitutions). Such substitutions are able to provide detailed information on the electronic structural consequences as a function of the functional group substitutions for CHBA.

The functional group substitution strategy on the electronic structure investigation of CHBA in this work is in gas phase, whereas the interactions with environment, such as aqueous solutions and other solvents, as well as detailed studies combined with synchrotron sourced experiments were presented elsewhere [13]. As we indicated before, there are no comprehensive results on the intrinsic electronic structures available for this class of benzene derivatives. It is important to understand the gas-phase information before we study their interactions with the environment so that we are able to differentiate what and how the environment impacts the properties. The present gas-phase quantum mechanical study will simulate and compare the geometrical and electronic properties, the infrared (IR) and Raman spectra, and the valence-to-core X-ray emission spectra and their changes as a function of the substitution patterns.

2 Computational details

All geometry optimizations were performed using the DFT-based B3LYP/cc-pVTZ model, which is incorporated in the GAMESS computational chemistry package [14], followed by harmonic vibrational frequency calculations using the Gaussian03 computational chemistry package [15]. This DFT-based model of B3LYP/cc-pVTZ possesses similar quality to the model of B3LYP/cc-pVTZ in our previous gas-phase dipeptide studies [13], in order to keep consistency when progressing to larger dipeptides consisting of aromatic rings such as our most recent phenylalanylphenylalanine dipeptide study [16].

The optimized geometries of the compounds are true minimum configurations without any imaginary frequencies. Infrared (IR) spectra and Raman spectra are produced using the wave function generated by the B3LYP/cc-pVTZ

model as the Raman spectral simulation is significantly more computer resource demanding if larger basis sets were employed. The errors are introduced by the smaller basis set are expected to be systematic for all the species and can be almost removed by a global shift, as it is the relative changes that are important in the present study. Solvent effects on the IR spectra of CHBA in either polar or non-polar solvents, i.e., carbon tetrachloride (CCl_4 , $\epsilon = 2.23$), dichloromethane (CH_2Cl_2 , $\epsilon = 8.93$) and water (H_2O , $\epsilon = 78.36$), are simulated using the polarizable continuum model (PCM) [17].

Hirshfeld charges [18, 19] and core ionization energies were calculated using the LB94/et-pVQZ//B3LYP/cc-pVTZ model [20, 21], which is incorporated in the Amsterdam Density Functional (ADF) computational chemistry package [22]. For core ionization energy calculations, the even tempered Slater basis set et-pVQZ is combined with the LB94 [20, 21] functional, the model (LB94/et-pVQZ) has been proven to produce accurate core ionization energies for a number of molecules with respect to the experiments [13, 23, 24]. The outer valence photoelectron spectroscopy of the benzene derivatives are produced using the outer valence Green function OVGf/6-311G**//B3LYP/cc-pVTZ model [25–30], which is available in the Gaussian03 package [15]. The cc-pVTZ and the larger 6-311++G** basis sets do not produce apparently different geometries for the species under study but with significantly different computer resources and obviously different ionization energies in the valence space. As a result, the more accurate OVGf/6-311++G** model is employed to improve the accuracy of the ionization energies in the outer valence space.

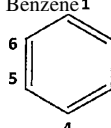
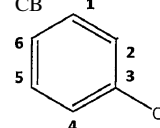
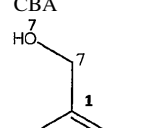
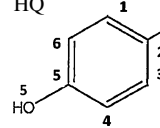
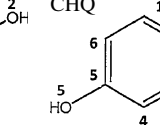
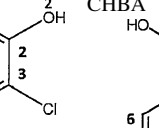
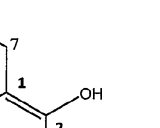
The ionization spectra are simulated using Gaussian broad function with the full width at half maximum (FWHM) of 0.04 eV for C(1)s and 0.10 eV for O(1)s spectra.

3 Results and discussion

3.1 Geometrical and other molecular properties

The optimized geometrical parameters and other molecular properties of 3-chloro-2,5-dihydroxybenzyl alcohol (CBHA) and its derivatives in Fig. 1 are presented in Table 1. The experimental geometrical data, which are available only for chlorobenzene (CB) and hydroquinone (HQ), are also presented in this table. The ring perimeter, R_6 , represents the perimeter of the benzene ring [31], μ is the dipole moment and $\langle R^2 \rangle$ is the electronic spatial extent, which describes the size of the molecule. The geometrical results agree well with the available experimental results of CB and HQ, but are slightly smaller than the respective experimental values. For example, both the

Table 1 Optimized geometric parameters of benzene derivatives in their electronic ground state

Properties	Benzene ¹		CB		CBA	HQ		CHQ	CHBA
									
	Cal. ^a	Exp. ^b	Cal. ^a	Exp. ^c	Cal. ^a	Cal. ^a	Exp. ^f	Cal. ^a	Cal. ^a
R ₆ (Å)	8.35	8.35	8.34	8.37	8.34	8.35	8.37	8.34	8.34
C(3)–Cl (Å)			1.73	1.73 ^d	1.75			1.75	1.76
C(1)–C(7) (Å)					1.51				1.51
C(2)–O(2) (Å)						1.38		1.37	1.37
C(5)–O(5) (Å)						1.38		1.37	1.37
C(7)–O(7) (Å)					1.42				1.42
∠C(6)C(1)C(2) (°)			120.39	120.24	119.26	121.31	120.0	120.93	119.07
∠C(2)C(3)C(4) (°)			120.41	121.65	121.27	118.75	119.9	121.83	122.06
∠C(3)C(4)C(5) (°)			119.58	119.04	118.68	121.31	120.0	119.28	118.75
∠C(5)C(6)C(1) (°)			119.64	119.78	120.28	118.75	119.9	120.30	121.31
∠C(6)C(1)C(2)C(3) (°)			0.00	0.00	−0.54	0.00		0.08	−0.24
∠C(1)C(2)C(3)C(4) (°)			0.00	0.00	0.46	0.00		−0.13	−0.04
∠C(4)C(5)O(5)H(5) (°)						180.00		−178.26	−179.35
μ (D)	0.00		1.75	1.60 ^e	0.66	0.00		1.60	1.61
<R ² > (a.u.)	457.58		894.90		1,682.84	950.06		1,422.39	2,132.27

^a The B3LYP/cc-pVTZ model^b Ref. [52]^c Ref. [53]^d Ref. [54]^e Ref. [55]^f Ref. [56]

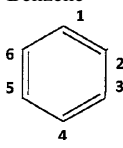
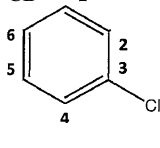
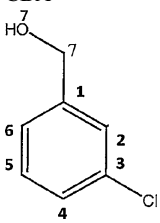
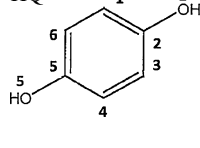
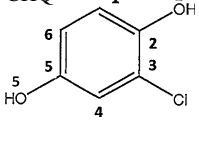
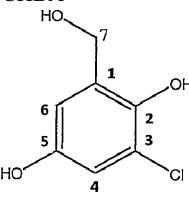
R₆ of CB and HQ derived from experiments are given by 8.37 Å, whereas this parameter is given by 8.34 Å for CB and 8.35 Å for HQ using our B3LYP/cc-pVTZ model.

The aromatic ring-related isotropic geometrical properties of the benzene derivatives, such as bond lengths and bond angles, exhibit subtle changes with respect to benzene. The perimeter of the benzene ring undergoes small changes, which indicates that substitutions of the hydrogen atoms by other functional groups do not alter the ring perimeter, as such substitutions do not involve any bond order changes in the benzene ring, which is also found from previous studies on biomolecules [13, 23, 32]. It seems that the C–Cl bond contributes to a subtle reduction in the perimeter of the chlorinated benzene derivatives. For example, the ring perimeters (R₆) of all chlorinated aromatic compounds in Table 1, i.e., CB, CBA, CHQ and CHBA, are the same, 8.34 Å, which is reduced by 0.01 Å from the ring perimeter of unsubstituted benzene of 8.35 Å

[31]. However, hydroquinone (HQ) does not involve any C–Cl bond and its ring perimeter remains as 8.35 Å, which is the same as that of unsubstituted benzene.

The C–Cl bond length increases with the number of substitutions among the four chlorinated benzene derivatives in Table 1. For example, the C–Cl bond length in chlorobenzene (CB) with one substitution at the C(3) position is 1.73 Å; the C–Cl bond length in 3-chlorobenzyl alcohol (CBA) with two substitutions at the C(1) and C(3) positions is 1.75 Å; the same C–Cl bond length in chlorohydroquinone (CHQ) with three substitutions at the C(2), C(3) and C(5) positions is 1.75 Å, and this C–Cl bond length in 3-chloro-2,5-dihydroxybenzyl alcohol (CHBA) with four substitutions at the C(1), C(2), C(3) and C(5) positions is given by 1.76 Å. This bond length of C–Cl increases 0.03 Å in CHBA from CB. The C–C–C bond angles of the benzene ring are relaxed by 1–2° in the vicinity of the 120° benzene D_{6h} point group symmetry due

Table 2 Hirshfeld charges of molecules calculated at LB94/et-pVQZ level of theory

Atomic site	Benzene	CB	CBA	HQ	CHQ	CHBA
						
C(1)	-0.044	-0.038	0.007	-0.059	-0.047	0.001
C(2)	-0.044	-0.054	-0.058	0.071	0.063	0.061
C(3)	-0.044	0.017	0.018	-0.051	0.004	0.006
C(4)	-0.044	-0.054	-0.056	-0.059	-0.064	-0.063
C(5)	-0.044	-0.038	-0.037	0.071	0.075	0.078
C(6)	-0.044	-0.043	-0.046	-0.051	-0.059	-0.057
C(7)			0.016			0.014
O(2)				-0.233	-0.229	-0.212
O(5)				-0.233	-0.226	-0.223
O(7)			-0.258			-0.272
Cl		-0.031	-0.039		-0.004	-0.003

to the functional group substitutions. Some C–C–C angles, such as $\angle C(2)C(3)C(4)$, are always larger than 120° , regardless the number of substitutions; other angles can be either larger or smaller than 120° , depending on the functional groups and the number of substitutions. However, the dihedral angles confining the planar structure of benzene become non-zero in CBA, CHQ and CHBA. For example, the $\angle C(6)C(1)C(2)C(3)$ angle is given by -0.54° in CBA, 0.08° in CHQ and -0.24° in CHBA.

The presence of electronegative groups, such as chlorine and hydroxymethyl attached to the *trans*-hydroquinone (HQ) fraction of the molecule, results in an increase in the dipole moment. The high symmetry of benzene (D_{6h}) and HQ (C_{2h}) leads to zero dipole moment of the compounds, and symmetric vibrations in their IR spectra can be inactive. The substitutions, when the high symmetry is broken, lead to non-zero dipole moments. Among the lower symmetry derivatives, the dipole moment of CBA is 0.66 D, whereas the dipole moment of CB, CHQ and CHBA are given by 1.75, 1.60 and 1.61 D, respectively. The electronic spatial extent ($\langle R^2 \rangle$) increases with the number of substitutions as shown in Table 1. For example, the unsubstituted benzene has the smallest electronic spatial extent of 457.58 a.u., whereas the $\langle R^2 \rangle$ of CHBA, which is the largest among the benzene derivatives in the present study, is given by 2132.27 a.u. The order of the $\langle R^2 \rangle$ exhibits as benzene $\langle CB \rangle < CBA \langle HQ \rangle < CHQ \langle CHBA$.

Table 2 provides the atomic site-dependent Hirshfeld charges (Q^H) [19, 20] on the non-hydrogen atoms of the

benzene derivatives. As a reference, the Q^H of the non-hydrogen atoms of benzene is also given in the same table. When the carbons bond with hydrogens, the Q^H of carbon atoms are negative to balance the positive charges of the hydrogen atoms. The functional groups such as chlorine, hydroxyl and hydroxymethyl, which are either directly bonded to a carbon atom in the ring, such as chlorine or hydroxyl, or indirectly bonded to a carbon atom like hydroxymethyl, are more electrophilic than the carbon atoms ($Q^H = -0.044$ a.u.) in benzene. As a result, the charges of the carbon atoms in the benzene ring, which bonds with the functional groups, have their signs changed from negative to positive in this table. For example, the Q^H on carbon site, C(3), in CB changes from -0.044 to 0.017 a.u. In fact, the charge distribution exhibits certain symmetry with respect to the axis through C(3) and C(6) in CB. For example, the Q^H on C(1) and C(5) of CB are the same, both are given by -0.038 a.u. Similarly, the Q^H on C(2) and C(4) of the same molecule are also the same as -0.054 a.u., as shown in Table 2. In CBA, it can be predicted that the substitutions happen on sites C(1) and C(3), as the Q^H of these sites becomes positively charged. In CHBA, the Q^H changes sign at C(1), C(2), C(3) and C(5) positions. The minor charge at C(1), i.e., 0.001 a.u., reveals that the hydroxymethyl carbon is nearly neutral. In Table 2, it also shows that the negative charges accumulated at the Cl sites have been significantly reduced in CHQ and CHBA, comparing to CB and CBA. This is due to the strong electrophilicity of the hydroxyl group(s) in CHQ and CHBA.

3.2 Vibrational spectroscopy

Among the six benzene derivatives, only the gas-phase experimental IR spectra of CB, CBA and HQ are available in the literature [33]. Figure 2a compares the simulated IR spectra (solid lines) of CB, CBA and HQ in the present study with available experimental IR spectra (dot lines) in gas phase. The IR spectra, which are simulated using the B3LYP/cc-pVTZ model, are scaled by 0.96 [34, 35]. Excellent agreement between the simulated and the experiment is achieved in this figure. The simulated spectra almost reproduce all details of important spectral peaks of the IR spectra for CB, CBA and HQ. This indicates that the B3LYP/cc-pVTZ model is able to produce accurate results for these benzene derivatives. This finding is in agreement with recent DFT functional performance assessment studies [36, 37] that the overall performance of the B3LYP method on a number of isotropic properties is consistently high, although not the best for a particular category. As a result, in the present study, we proceed to simulate the IR spectra of all the benzene derivatives using the B3LYP/cc-pVTZ model, in order to make a consistent comparison.

Figure 2b reports the simulated IR spectra of all six compounds. In general, the IR spectra can be divided into three major frequency regions, that is, Band I of 500–1,600 cm^{-1} , Band II of 2,800–3,100 cm^{-1} and Band III of 3,500–3,800 cm^{-1} . The frequencies in a particular region are attributed to different solitary and/or combined vibrational modes. What are in common for all the IR spectra in Fig. 2b is the ring stretch and C–H stretch vibrations. Their spectral positions either shift such as ring stretches or split, such as the C–H stretches due to the substitutions. The C–Cl stretch vibrations only exist in those with the Cl substitution and the O–H stretch peaks exist in the OH substitutions.

Band I in the low-frequency region is related to bend and rock vibrations of C–C, C–H, C–Cl, C–O, C=C, O–H and aromatic C–C ring motions. The O–H bending of phenolic hydroxyl groups in hydroquinone and its substitutes (e.g., CHQ and CHBA) are highlighted in the spectra by a prominent peak at ca. 1,150 cm^{-1} , which is characteristic to this group of molecules [38–40]. The IR spectra of benzene and CB reveal the impact of the addition of the Cl atom in CB. However, not all the spectral peaks of CB are due to the Cl-related vibrations. Some symmetric vibrations, which are inactive in benzene, become IR active in CB due to its symmetry breaking. Because of the increase in the number of substitutions, the peaks in the Band I (e.g., 500–1,600 cm^{-1}) become more complex.

The C–Cl stretch vibration frequency in Band I exhibits a blueshift with respect to the $\nu_{\text{C-Cl}}$ of CB, depending on the functional groups and their position on the phenol ring. For example, the $\nu_{\text{C-Cl}}$ of both CBA and CHBA are both

given by 822 cm^{-1} from the present model, which blueshifts approximately 140 cm^{-1} from the $\nu_{\text{C-Cl}}$ of CB, whereas the $\nu_{\text{C-Cl}}$ of CHQ blueshifts only 77 cm^{-1} from that of CB. This may be due to the intramolecular hydrogen bonds in the benzene derivatives. The benzene derivatives with a chlorine exhibit a Cl···H(4) distance of 2.85 Å for CB, 2.84 Å for CBA, 2.87 Å for CHQ and 2.88 Å for CHBA, which are in the vicinity of hydrogen bond interaction region of 2.80 Å [41]. It is also noted that in CHBA the Cl···H(2) distance is even shorter, at 2.26 Å. In addition, CBA and CHBA exhibit similarly large C–Cl stretch blueshifts in their IR spectra, which are caused by the unique hydrogen bond network as well as the large van der Waals (vdW) radii of chlorine in this molecule pair. As shown in Fig. 1b and c, in CBA, the distance between O(7)···H(6)–C(6) is given by 2.59 Å, whereas in CHBA, the distance between O(7)–H(7)···O(2)–H(2) is given by 2.24 Å and the distance between C(7)–H'(7)···O(2)–H(2) is given by 2.77 Å. These hydrogen bonds are within the hydrogen bond cutoff criterion of 2.80 Å [38] and form a hydrogen bond network in CHBA.

Band II at about 3,000 cm^{-1} corresponds to the C–H stretch vibrations, which splits into three peaks in both CBA and CHBA and becomes significantly weaker when the number of substitutions in the compounds increases. For example, the small IR peaks in this frequency region for CHBA (four substitutions) are apparently smaller than the peaks in the similar frequency region for CBA (two substitutions). A single peak in Band II at 3,075–3,050 cm^{-1} of benzene and CB is attributed to the ring C–H stretch vibrations. This peak significantly reduces its intensity in HQ and CHQ but splits into three peaks with redshift in the spectra of CBA and CHBA. The former, the reduced intensities, are due to the dipole moment changes and the increasing degree of substitutions, which reduce the number of ring C–H bonds in the molecules and lead to low C–H stretch intensities. The latter, the split IR peaks, indicates that the C–H stretch splitting in CBA and CHBA can be due to the “through space” hydrogen bond interactions in the hydrogen bond network indicated above. The hydrogen atom in the CH₂ group of hydroxymethyl in CBA and CHBA promotes the complexity of the C–H stretch vibrations in both the IR (and Raman) spectra of the molecule pair.

Band III in the spectral region of ca. 3,600 cm^{-1} is dominated by the O–H stretch vibrations, which depend on the molecular dipole moment, the number of the OH groups and their chemical environment. For example, an OH stretch vibration of the hydroxymethyl side chain will be weaker in the intensity than that of the OH stretch in HQ, which possesses two identical OH groups due to symmetry. The O–H stretch peak splits in CHBA and CHQ, however. The combined impact of the chlorine group and the hydroxymethyl

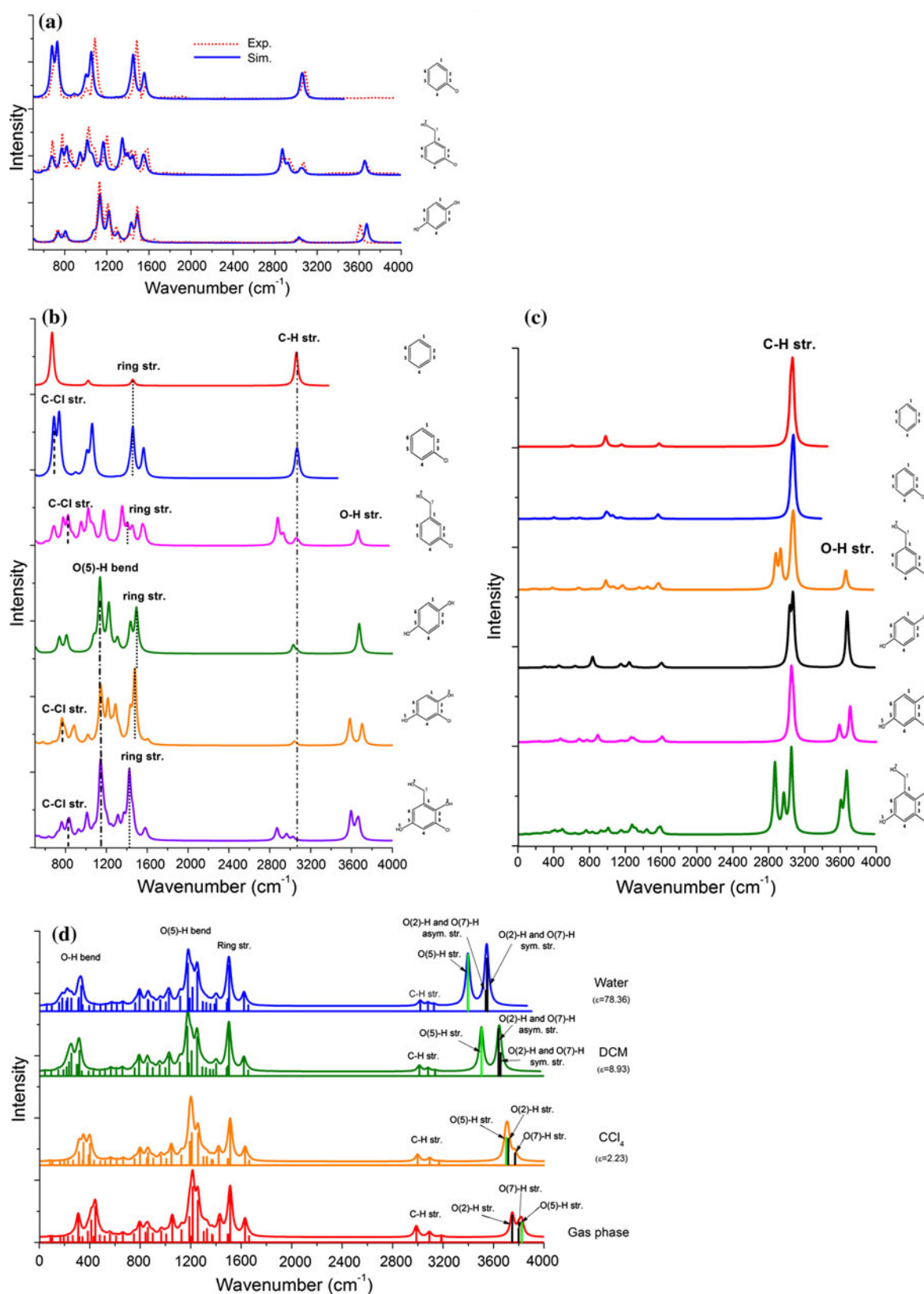


Fig. 2 **a** Comparison of the simulated IR spectra (*solid lines*) with available experimental IR spectra (*dotted line*) of CB, CBA and HQ. **b** Comparison of the simulated IR spectra. **c** Simulated Raman spectra

of benzene, CB, CBA, HQ, CHQ and CHBA using the B3LYP/cc-pTVZ model and **d** Solvent effects on the IR spectra of CHBA with respect to gas phase

group to the electronic structure and dipole moment of CHBA is different from that of chlorine alone on CHQ. As a result, in CHQ, the O(2)–H stretch blueshifts about 90 cm^{-1} but the O(5)–H stretch redshifts 30 cm^{-1} with respect to the HQ counterpart. The hydroxymethyl group in CHBA helps to reduce the O–H differences and results in less split peaks in this spectral band.

Bands II and III for the C–H stretch and O–H stretch vibrations may be well elucidated by the Raman spectra, which are given in Fig. 2c. Like the IR spectra given by Fig. 2b, the same scaling factor of 0.96 is applied. It is apparent that the O–H stretch modes of the OH (hydroxyl) groups that are attached to the phenyl ring (HQ, CHQ, and CHBA) exhibit more intense Raman scattering than that of the O–H stretch mode of the OH (hydroxyl) group that is attached to the methylene carbon in CBA. The chlorine at the C(3) position of the phenyl ring of CHQ and CHBA certainly affects the OH stretch vibrations through the hydrogen bond with H(2) and H(4). It is interesting that chlorine in CB and CHQ does not seem to affect the C–H ring stretch vibrations in these compounds; however, when an additional hydroxymethyl group is bonded to the aromatic ring, as in CBA and CHBA, the C–H stretch peaks split, as obviously seen in Fig. 2c.

Solvents affect the vibrational spectra of molecules [42, 43]. Figure 2d provides the simulated IR spectra of CHBA under either polar (water $\epsilon = 78.36$ and dichloromethane (DCM), $\epsilon = 8.93$) or non-polar (e.g., tetrachloromethane (CCl_4), $\epsilon = 2.23$) solvents using the polarizable continuum model (PCM) model with respect to the IR spectrum in gas phase. The possible systematic errors in the simulated IR spectra introduced by the B3LYP/cc-pVTZ model are expected to be minor. As a result, differences appear in the IR spectra for CHBA can be considered as being caused by the solvent effects. As can be seen in this figure, the most obvious spectral changes caused by solvent effects are the IR redshifts in the regions of ca. $300\text{--}400\text{ cm}^{-1}$ and ca. $3,500\text{--}3,900\text{ cm}^{-1}$. The far-IR region ($300\text{--}400\text{ cm}^{-1}$) is responsible for the O–H bending vibrations whereas the high-IR region ($3,500\text{--}3,900\text{ cm}^{-1}$) is responsible for the O–H stretch vibrations (the mid-IR is normally considered to be between 800 and 1600 cm^{-1} , and not 3500 and 3900 cm^{-1}). There is a general trend of redshift of the IR spectra in solutions with respect to the gas phase: the redshifts increase with the increase in the solvent dielectric constant, ϵ , that is, the larger the dielectric constant of the solvent (i.e., the more polar the solvent), the more apparent the redshifts in the IR spectra, in both regions.

The impact of the solvent effects in the two IR regions of CHBA is not the same. The amplitudes of the redshift with respect to the IR in gas phase in the far-IR region of $300\text{--}400\text{ cm}^{-1}$ are less significant than the shift in the high-IR region of $3,500\text{--}3,900\text{ cm}^{-1}$. For example, the largest redshift

in the $300\text{--}400\text{ cm}^{-1}$ is in water, with an approximately 100 cm^{-1} redshift, whereas in the non-polar tetrachloromethane solvent, the redshift is even smaller. However, the intensities of the spectral bands are not apparently different from the band in the gas phase in this region. On the other hand, solvents apparently enhance the redshift in the higher-frequency region of $3,500\text{--}3,900\text{ cm}^{-1}$ of CHBA, both in frequency and in intensity, which obviously depends on the polarity of the solvents. For example, the redshift in aqueous solution (water) is the most significant among the three solvents with respect to the amplitude of the shift and the band intensity; a band with an over 350 cm^{-1} redshift in frequency and an over three times larger intensity is observed. Moreover, the reaction of the O–H groups of CHBA to the solvents is quite different, too. In the gas phase, the O(2)–H stretch frequency is smaller than that of the O(5)–H and O(7)–H stretch frequencies, which are closer in positions, that is, $\nu(\text{O}(2)\text{--H}) < \nu(\text{O}(7)\text{--H}), \nu(\text{O}(5)\text{--H})$. When in solution, the smallest O(5)–H stretch frequency in gas phase becomes the largest among the O–H stretch bands, regardless the polarity of the solvents.

The redshift of the $\nu(\text{O}(5)\text{--H})$ IR band (marked as green spectral line in the figure) is more significant than other O–H stretch bands such as $\nu(\text{O}(2)\text{--H})$ and $\nu(\text{O}(7)\text{--H})$, which also depends on the polarity, i.e., dielectric constant of the solvents, for example, $\Delta\nu(\text{O}(5)\text{--H})$ in CCl_4 ($\epsilon = 2.23$), $<\Delta\nu(\text{O}(5)\text{--H})$ in DCM ($\epsilon = 8.93$) and $<\Delta\nu(\text{O}(5)\text{--H})$ in water ($\epsilon = 78.36$). The redshifts of $\Delta\nu(\text{O}(2)\text{--H})$ and $\Delta\nu(\text{O}(7)\text{--H})$ are relatively small with respect to their gas-phase positions. This might indicate that the O(5)–H group is more significantly affected by the hydrogen bond network with the polar solvents of water and DCM than its O(2)–H and O(7)–H counterparts as both solvents contain hydrogen atoms.

It is also found that the relative spectral line positions of $\nu(\text{O}(2)\text{--H})$ and $\nu(\text{O}(7)\text{--H})$ also depend on the polarity of the solvents: in non-polar solvent, such as tetrachloromethane (CCl_4), $\nu(\text{O}(2)\text{--H}) > \nu(\text{O}(7)\text{--H})$, and $\nu(\text{O}(2)\text{--H})$ and $\nu(\text{O}(7)\text{--H})$ exhibit a larger splitting in frequencies, whereas in polar solvents, such as water and dichloromethane (DCM), $\nu(\text{O}(2)\text{--H}) \sim \nu(\text{O}(7)\text{--H})$. However, the observations of the behavior of the O–H group in CHBA in solvents are hardly generalized as more comprehensive studies on solvents with various polarity with and without hydrogen atoms are warranted for a generalized conclusion, which is out of the scope of the present study.

3.3 Vertical core ionization spectra

Table 2 reports the vertical core binding energies of the benzene derivatives calculated using the LB94/et-pVQZ model under the “meta-Koopman” theorem [44]. The calculated core binding energies of CB and HQ are also compared with available experimental results in the same

table. For the binding energies of CB, due to the instrumental resolution, etc., the experiment has measured only two carbon core C–K energies [45]. That is, the binding energy of C(3), which bonds with chlorine, is given by 287.1 eV, and is approximately 1.4 eV different from the other aromatic carbons which have binding energies of 285.7 eV [46]. The experiment was unable to measure the

subtle energy differences among the aromatic carbons in CB. Similarly, the experimental results for HQ also resulted in two sets of binding energies for the aromatic carbons [47]. That is, 287.1 eV for C(2) and C(5) sites, which respectively bond with the hydroxyl groups. The binding energies for other aromatic carbons are the same, i.e., all at 285.7 eV. If we apply a global energy shift of 4.182 eV to

Fig. 3 Comparison of the simulated vertical core ionization C–K spectra (a) and O–K spectra (b) of the benzene derivatives

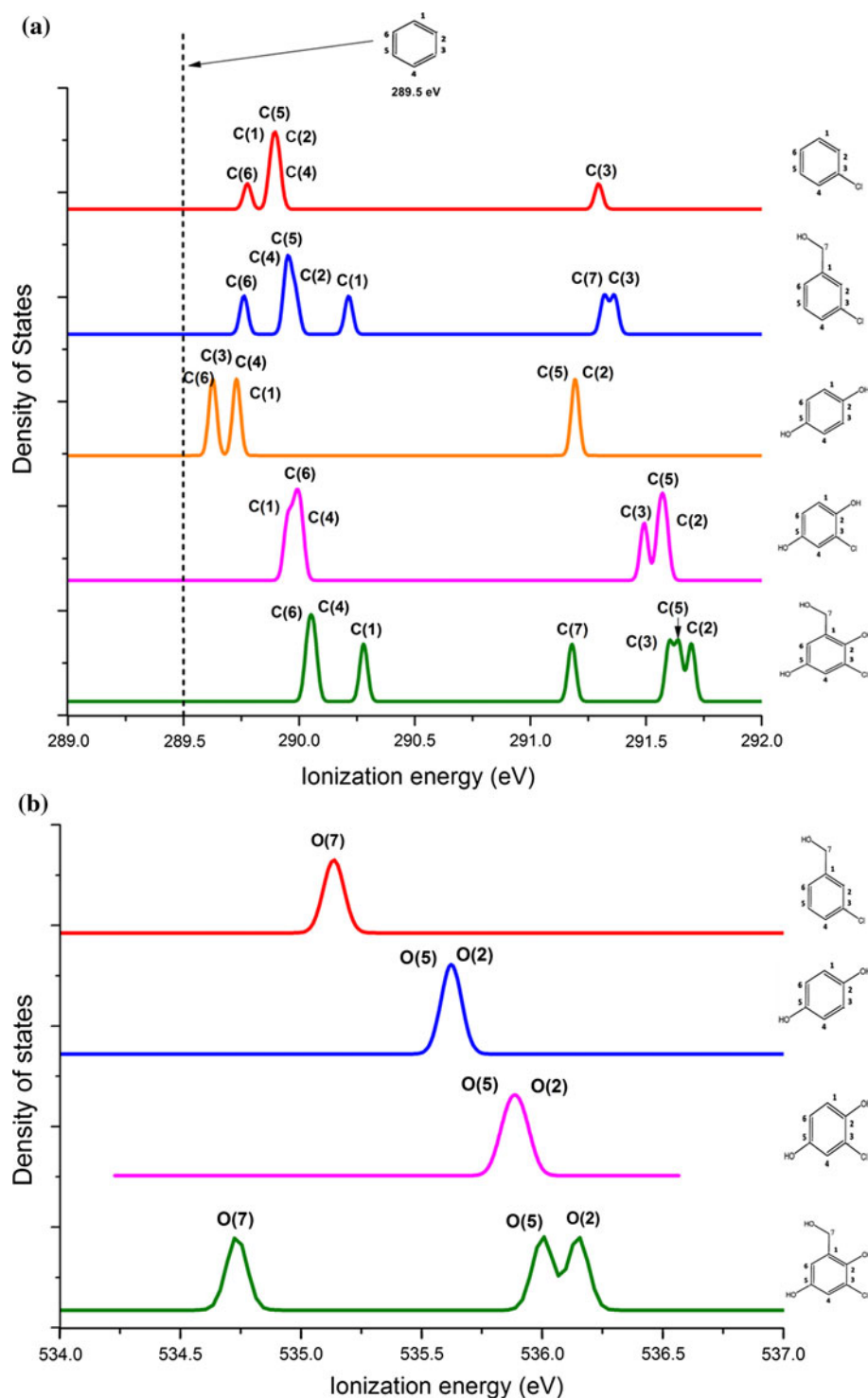


Table 3 Comparison of calculated vertical C–K and O–K ionization energies with available experimental energies (eV)

Site	Benzene		CB		CBA	HQ		CHQ	CHBA
	Cal. ^a	Exp. ^{b, c}	Cal. ^a	Exp. ^d	Cal. ^a	Cal. ^a	Exp. ^e	Cal. ^a	Cal. ^a
C(1)	289.5	290.42	289.882	285.7	290.214	289.729	285.7	289.949	290.279
C(2)	289.5	290.42	289.908	285.7	289.984	291.193	287.0	291.583	291.696
C(3)	289.5	290.42	291.295	287.1	291.363	289.626	285.7	291.492	291.600
C(4)	289.5	290.42	289.908	285.7	289.944	289.729	285.7	290.006	290.064
C(5)	289.5	290.42	289.882	285.7	289.954	291.193	287.0	291.558	291.641
C(6)	289.5	290.42	289.775	285.7	289.761	289.626	285.7	289.982	290.039
C(7)					291.319				291.179
O(2)						535.623		535.916	536.146
O(5)						535.623		535.858	535.999
O(7)					535.136				534.731

^a Using the LB94/et-pVQZ model

^b Ref. [57]

^c Ref. [58]

^d Ref. [46]

^e Ref. [47]

CB in order to reduce the systematic error introduced by the model, the agreement with experiment is very good. Note that the global energy shift to HQ [47] is 4.029 eV, and both experiments [43, 44] are unable to provide the binding energies for the oxygen atoms in CB and HQ. For the only two available core binding energies of chlorine in CB [46], a larger energy shift of 5.227 eV applies. Again, the experiment [46] could not differentiate the energy difference between $Cl_{2p_{1/2}}$ and $Cl_{2p_{3/2}}$.

Figure 3a presents the simulated carbon C–K binding energy spectra using a full width at half maximum (FWHM) of 0.04 eV for the compounds. The vertical dashed line in the spectra marks the position of the C–K of benzene at 289.50 eV using the same model. As seen in this figure, all the C(1)s binding energies of the ring carbons of these benzene derivatives are shifted to higher energy in the spectra, indicating that the functional group substitution possibly stabilizes the benzene derivatives. The C–K spectra of the benzene derivatives split significantly into two groups, the splitting being approximately 1 eV and depending on the chemical environment. Starting with CB, the C(1)s binding energy of the C(3) carbon atom when connected to a functional group, for example, Cl, becomes apparently higher, suggesting that the C(1)s electrons of this carbon are then more difficult to ionize. As a result, the C–K binding energy peaks at higher energy in the spectra correspond to the carbon atoms that are bonded to a more negative atom or group. For example, the C(1)s binding energies of the C(2), C(5) and C(6) carbons are located at higher energy in the C–K binding energy spectra of CHQ, which indicates that the C(2) and C(5) atoms may

bond with similar functional groups with more negative Hirshfeld charges than these carbon atoms. The C(3) site bonds with a different atom or group, which also has more negative Hirshfeld charge than carbon.

The spectral peak of the C(1) carbon in CBA and CHBA does not move to higher energy as significantly as do the spectral peaks of other carbon atoms with substitutions since the hydroxyl in hydroxymethyl is bonded not directly to the phenyl ring at C(1), but to the methylene carbon C(7). The position of the peak corresponding to C(7) carbon in CBA and CHBA is unique. In CBA, the C(7) carbon atom is bonded to the C(1) phenyl ring carbon on one side and the hydroxyl O(7) oxygen on the other side. Its C–K spectral peak has a very similar C(1)s binding energy value to that of the C(3) carbon atom that is bonded to the Cl atom, while in CHBA, the spectral peaks corresponding to the C(1)s binding energies of the C(7) and C(3) atoms split by approximately 0.4 eV (refer to Table 3). As CHBA also has hydroxyl groups bonded to the C(2) and C(4) carbon atoms, the compound certainly forms a very different interaction network which includes the hydroxymethyl group and the chlorine atom at the *meta* positions to each other in the phenyl ring. As noted before, the hydrogen bond networks in CBA and CHBA may also contribute to changes in their C–K binding energy spectra.

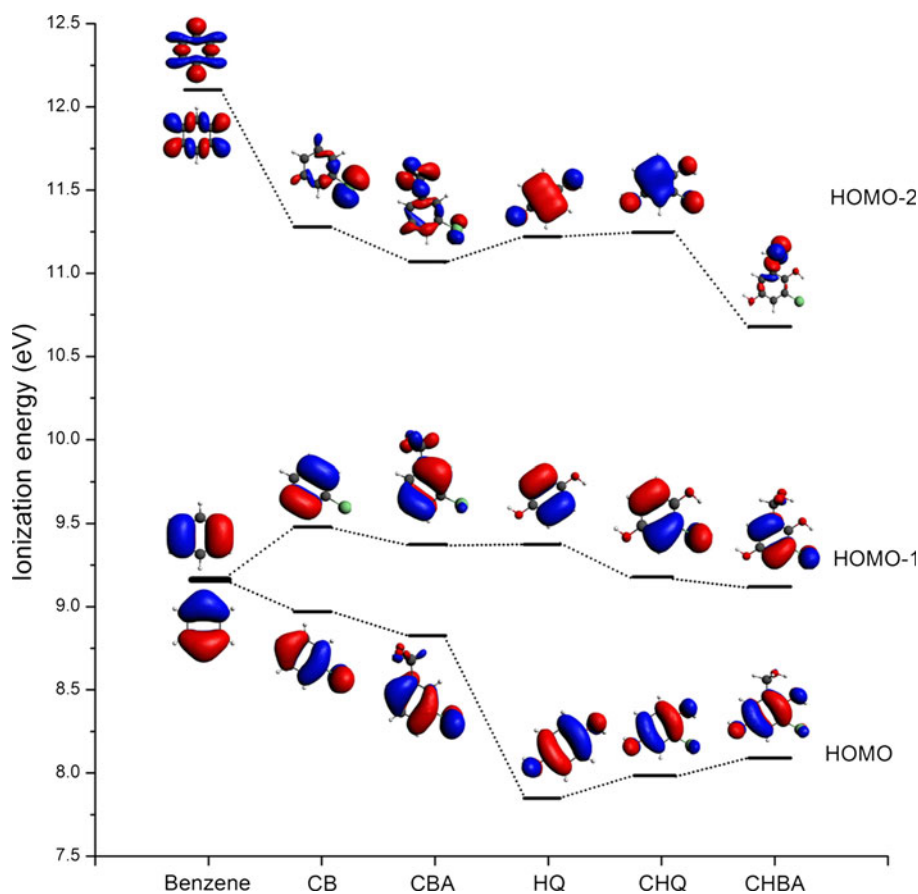
Figure 3b presents the simulated O–K binding energy spectra for the four hydroxyl group containing compounds, that is, CBA, HQ, CHQ and CHBA. The O–K spectra of CHA, HQ and CHQ exhibit a single spectral peak, whereas three peaks are seen in the O–K spectra of CHBA. These features can be related to the structures of these

Table 4 Outer valence (IP < 20 eV) vertical ionization energies of the benzene derivatives

Orb.	Benzene		Orb.	CB		Orb.	CBA		Orb.	HQ		Orb.	CHQ		Orb. no.	CHBA	
	Exp. ^a	OVGF ^d		Exp. ^b	OVGF ^d		Exp. ^c	OVGF ^d		Exp. ^c	OVGF ^d						
1e _{1g}	9.2	9.16 (0.90)	4b ₁	9.08	8.97 (0.90)	37a	8.83 (0.90)	3b _g	8.44	7.85 (0.90)	37a	7.99 (0.90)	45a	8.10 (0.90)			
3e _{2g}	11.5	12.10 (0.90)	1a ₂	9.7	9.48 (0.90)	36a	9.38 (0.89)	2b _g	9.66	9.38 (0.90)	36a	9.18 (0.90)	44a	9.12 (0.89)			
1a _{2u}	12.3	12.36 (0.81)	9b ₂	11.33	11.28 (0.90)	35a	11.08 (0.90)	2a _u	11.21	11.22 (0.85)	35a	11.25 (0.86)	43a	10.68 (0.90)			
3e _{1u}	13.9	14.44 (0.88)	3b ₁	11.66	11.73 (0.88)	34a	11.39 (0.89)	12a _g	11.98	12.16 (0.90)	34a	11.82 (0.90)	42a	11.25 (0.87)			
1b _{1u}	15.5	14.83 (0.87)	15a ₁	12.25	12.60 (0.90)	33a	11.61 (0.89)	11a _g	12.31	13.36 (0.90)	33a	12.43 (0.90)	41a	11.93 (0.90)			
2b _{2u}	14.8	15.79 (0.86)	8b ₂	13.0	12.63 (0.90)	32a	12.27 (0.90)	12b _u	12.74	13.33 (0.90)	32a	12.67 (0.88)	39a	12.32 (0.90)			
3a _{1g}	16.9	17.37 (0.85)	2b ₁	13.17	13.35 (0.83)	31a	12.69 (0.90)	1b _g	13.56	13.87 (0.89)	31a	13.57 (0.90)	38a	12.79 (0.88)			
2e _{2g}	19.2		14a ₁	14.27	14.64 (0.88)	30a	13.24 (0.86)	1a _u	14.37	14.30 (0.83)	30a	13.92 (0.90)	37a	13.16 (0.90)			
			7b ₂	14.60	14.78 (0.88)	29a	13.40 (0.87)	11b _u	14.37	14.68 (0.88)	29a	14.19 (0.89)	36a	13.56 (0.90)			
			6b ₂	15.31	15.49 (0.87)	28a	14.59 (0.88)	10b _u	16.05	15.14 (0.88)	28a	14.81 (0.89)	35a	14.08 (0.90)			
			13a ₁	15.7	15.99 (0.87)	27a	14.80 (0.89)	10a _g	16.05	15.25 (0.89)	27a	14.72 (0.82)	34a	14.34 (0.88)			
			12a ₁	16.91	17.47 (0.85)	26a	15.38 (0.88)	9b _u	17.53	16.13 (0.88)	26a	15.34 (0.88)	33a	14.91 (0.90)			
						25a	15.50 (0.88)				25a	15.56 (0.89)	32a	14.92 (0.88)			
						24a	15.97 (0.87)				24a	16.54 (0.88)	31a	14.98 (0.85)			
						23a	17.20 (0.88)				23a	17.86 (1.29)	30a	15.35 (0.85)			
						22a	17.53 (0.86)				22a		29a	15.72 (0.89)			
													28a	16.62 (0.89)			
													27a	17.26 (0.89)			

^a Ref. [49]^b Ref. [50]^c Ref. [51]^d The basis set used is 6-311++G** and the pole strength values of OVGF are in parentheses

Fig. 4 Valence ionization energy diagram of the frontier orbitals, i.e., HOMO, HOMO-1 and HOMO-2 of the benzene derivatives



compounds. In CHA, there is only one hydroxyl group, which simply results in a single O–K peak at 535.136 eV in the spectrum. The single O–K spectral peak at 535.623 eV represents the identical O(2) and O(5) oxygen atoms in HQ due to its high point group symmetry. The result of the presence of chlorine in CHQ is to shift the single binding energy peak from 535.136 eV of HQ to a slightly higher energy and to split the binding energies of O(2) and O(5) by 0.058 eV. Because the O(2) and O(5) oxygen atoms in CHQ are not equivalent anymore, the addition of Cl reduces the point group symmetry of CHQ. However, the energy resolution (FWHM) is insufficient to show two peaks. The additional hydroxymethyl group at the C(1) position of CHBA further enhances the differences between O(2) and O(5) so that their binding energies split even further to 0.15 eV, which is sufficient to present two peaks in the spectrum. In return, the interactions caused by the hydroxyl groups at C(2) and C(5) result in a lower binding energy for O(7) of CHBA.

3.4 Valence ionization spectra and chemical bonding

Valence orbitals, in particular frontier orbitals including the highest occupied molecular orbital (HOMO) of the aromatic molecules, provide useful information on chemical bonding

mechanism to our understanding of their structural behavior, which has been detailed by the Fukui frontier orbital theory [48]. As a result, in the present study, the valence ionization energy spectra of the benzene derivatives are simulated, together with frontier orbitals, such as HOMO, HOMO-1 and HOMO-2, which are studied in detail to explore the substitution effects. Table 4 lists the calculated vertical valence ionization potentials (IPs) of the compounds using the OVGF/6-311++G**//B3LYP/cc-pVTZ model, which are compared with available experimental IPs of benzene [49], chlorobenzene (CB) [50] and hydroquinone (HQ) [51]. In this model, only the binding energies with the spectroscopic pole strengths (PS) larger than 0.82 are given in this table. The calculated vertical IPs of the molecules agree fairly well with the available measurements in the outer valence space (IP < 20 eV) in benzene, chlorobenzene (CB) and hydroquinone (HQ).

To further understand the relationship between spectra and structures in outer valence space, it is useful to examine their frontier orbitals, that is, the highest occupied molecular orbital (HOMO), the next HOMO (HOMO-1) and the third HOMO (HOMO-2) of the molecules. Figure 4 provides an ionization energy diagram of the frontier orbitals and the orbital electron density distributions. In general, the substitutions to the phenyl hydrogens in

benzene reduce the ionization energies of the HOMOs and HOMO-2 but slightly increase the ionization energies of HOMO-1, as shown in Fig. 4. Subtle energy reductions are observed in CB and CBA by 0.23 and 0.37 eV, respectively, whereas a significant energy reduction by as much as 1.35 eV is observed in the HOMO of HQ with respect to benzene. However, the first IP reductions of CHQ and CHBA are given by 1.21 and 1.11 eV, respectively, with respect to the first IPs of benzene, which are 0.14 and 0.25 eV, respectively, higher than the first IPs of HQ, which is the lowest HOMO IP in this figure. On the contrary, the IPs of the HOMO-1 orbitals of the compounds increase with an energy less than 0.5 eV with respect to the HOMO-1 IP of unsubstituted benzene.

The trends of energy changes in the HOMO and HOMO-1 of the benzene derivatives are apparent. However, the electron density distributions of the orbitals change less significantly. As shown in Fig. 4, all the derivatives exhibit IP energy splittings of the HOMO and HOMO-1 that are the doubly degenerate HOMO and HOMO-1 of benzene, $1e_{1g}$. The orbitals (i.e., electron density distributions) of the orbital pairs in the derivatives remain more or less a similar pattern to those of benzene but the nodal planes are dependent on the substituting functional groups. For example, the HOMOs manage to retain a pattern of two nodal planes: one through the plane of the phenyl ring atoms, while the other is perpendicular to the phenyl plane, indicating that the HOMOs and HOMO-1s are dominated by $2p_z$ electrons of the phenyl carbons.

In the HOMOs, the perpendicular plane cuts through two pair of phenyl C–C bonds, dividing the electron density into a positive group and a negative group with three ring carbons in each group. This nodal plane differentiates CB and CBA from the others benzene derivatives in the study. For example, in the HOMOs, this nodal plane is through the middle of the C(1)–C(2) and C(4)–C(5) bonds in CB and CBA, whereas this plane is through the middle of the C(3)–C(4) and C(6)–C(1) bonds in HQ, CHQ and CHBA. No hydroxyl group(s) directly bonds with any phenyl carbons in CB and CBA, and the C(3) site does not involve with the C–C bonds associated with the perpendicular nodal plane. For example, the HOMOs of CB and CBA are grouped as C(2)–C(3)–C(4) for one sign and C(1)–C(6)–C(5) for the opposite sign. However, although the orbital electron density distributions of the HOMOs of HQ, CHQ and CHBA exhibit similar pattern as of CB and CBA, the orbital grouping becomes C(1)–C(2)–C(3) for one sign and C(4)–C(5)–C(6) for the opposite sign. In addition, the Cl atom in the HOMOs of CB and CBA is populated, but is not populated in the HOMOs of CHQ and CHBA.

The perpendicular nodal planes of the HOMO-1 orbitals cut through the axis formed by the two phenyl atoms rather than by two bonds as in the HOMOs. As a result, the

HOMO-1 orbitals are formed by the $2p_z$ electrons of two pairs of carbon atoms with each pair consisting of two rather than three carbon atoms as shown in Fig. 4. The IP energy differences in the HOMO-1 orbitals of the derivatives are not as significant as the HOMOs, although the perpendicular nodal plane of the HOMO-1 orbitals exhibits a similar pattern to the HOMOs. For example, both the HOMO-1 orbitals of CB and CBA have a nodal plane through the C(6)–C(3) axis and C(3) bonds with Cl. The HOMO-1 orbitals exhibit groupings of densities consisting of C(1)–C(2) and C(4)–C(5), whereas all atoms connecting with the C(6) and C(3) sites do not contribute significantly to the bonding. However, this nodal plane in HQ, CHQ and CHBA is through the (O(2)–C(2)–C(5)–O(5)) axis and the groupings of the densities are consisting of C(6)–C(1) and C(3)–C(4). Again, all the atoms connecting with C(6) and C(3) do not apparently contribute to the bonding in HQ, CHQ and CHBA. As a result, the substitutions and the functional groups do not make a large difference in their IPs of the HOMO-1 orbitals.

If the HOMO and HOMO-1 orbitals of the benzene derivatives exhibit certain similarities, the HOMO-2 orbitals are the orbitals that demonstrate individual bonding characters with respect to the substitutions. Unlike the HOMOs and HOMO-1 orbitals, none of the HOMO-2 orbitals of the derivatives exhibits similar electron density distribution to the antibonding character of the $3e_{2g}$ orbital of benzene. For example, the $9b_2$ orbital of CB concentrates on the Cl atom, whereas the 35a orbital of CBA on the hydroxymethyl chain. The $2a_u$ orbital of HQ is on the phenyl ring for a large- π bond, whereas the oxygen atoms of the hydroxyl groups possess opposite sign. The Cl–C(3) bond of the 35a orbital of CHQ breaks the large- π bonding structure in HQ, and the 43a orbital of CHBA is the only one where the hydroxymethyl chain is dominant. All of these HOMO-2 orbitals in the derivatives do not share similarities with the $3e_{2g}$ orbitals of benzene.

4 Conclusions

The electronic structure and chemical bonding of a bioactive compound, 3-chloro-2,5-dihydroxybenzyl alcohol (CHBA), are studied using simulated infrared (IR) and Raman spectroscopy, as well as core and valence vertical ionization spectra, through a comparison with a number of related bioactive benzene derivatives. Quantum mechanical models are employed in order to calculate the structures and to simulate the spectra. It is found that the C–H stretch vibration band at ca. $3,000\text{ cm}^{-1}$ and the O–H stretch vibration band at ca. $3,600\text{ cm}^{-1}$ in the IR and the Raman spectra differentiate the hydroxymethyl group and the hydroxyl groups, respectively, of CHBA from other

compounds in the study. Solvent affects the vibrational spectra of CHBA apparently on both ends of the 400–4,000 cm^{-1} region particularly in the higher-frequency region, depending on the polarity. The larger the dielectric constants of the solvent, the larger the redshift in frequency, and intensity is observed with respect to the gas-phase spectra. The fact that the O(5)–H hydroxyl group of CHBA exhibits a significant redshift in polar solvents may be due to its unique hydrogen bond network formed. The vertical core binding energy spectra clearly reveal that the chemical environment changes due to substitutions to binding energies of the carbon as well as the oxygen atoms. Intramolecular hydrogen bond network associated with CHBA plays an important role in its structure.

The valence ionization spectra of the benzene derivatives are more complex. The frontier orbitals exhibit apparent energy differences, reflecting the substitutions. The highest occupied molecular orbitals (HOMOs) exhibit a trend of ionization energy reduction from the HOMO of benzene, whereas the energies of HOMO-1 orbitals fluctuate and show small energy increases with respect to HOMO-1 of benzene. The orbital densities of the HOMO and HOMO-1 orbitals exhibits certain trends that they inherit from the corresponding orbitals of unsubstituted benzene. The third orbitals, HOMO-2s of the derivatives, serve as the signature of the derivatives, as it is unique in individual compounds. This orbital of CHBA possesses the lowest ionization potential with a unique hydroxymethyl dominant bonding.

Acknowledgments This paper is dedicated to Professor A. Imamura on the occasion of his 77th birthday in 2011, which coincides with the International Year of Chemistry. FW would like to thank Prof. Y. Aoki for her kind invitation to contribute to this special issue. The project is supported by the Australian Research Council (ARC). National Computational Infrastructure (NCI) at the Australian National University for the award under the Merit Allocation Scheme, Victorian Partnership for Advanced Computing (VPAC) and Swinburne University Supercomputing Facilities are acknowledged. APWA acknowledges the Swinburne University Centenary Postgraduate Research Award.

References

- Chen Y-PP, Ivanova EP, Wang F, Carloni P (2010) Bioinformatics. In: Mander L, Lui H-W (eds) In comprehensive natural products II chemistry and biology, vol 9. Elsevier, Oxford, p 569
- Butler MS (2005) Nat Prod Rep 22:162
- Chin Y-W, Balaunas MJ, Chai HB, Kinghorn AD (2006) AAPS J 8:E239
- Harvey AL (2007) Curr Opin Chem Biol 11:480
- Kwong TF, Miao L, Li X, Qian PY (2006) Marine Biotechnol 8:634
- Sequin-Frey M, Tamm C (1971) Helv Chim Acta 54:84
- McCorkindale NJ, Roy TP, Hutchinson SA (1972) Tetrahedron 28:1107
- Sakamura S, Ito J, Sakai R (1971) Agr Biol Chem 35:105
- Zhang Y, Ahn EY, Jiang Y, Kim DK, Kang SG, Wu C, Kang SW, Park JS, Son BW, Jung JH (2007) Int J Oncol 31:1317
- Zhang H, Xie H, Qiu SX, Xue J, Wei X (2008) Biosci Biotechnol Biochem 72:1746
- Wood EJ (2006) In: Crowe J, Bradshaw T, Monk P (eds) Chemistry for the biosciences: the essential concepts. Oxford University Press, Oxford, p 594
- Hoffmann R, Imamura A, Hehre WJ (1968) J Am Chem Soc 90:1499
- Wickrama Arachchilage AP, Wang F, Feyer V, Plekan O, Prince KC (2010) J Chem Phys 133:174319
- Schmidt MW, Baldrige KK, Boatz JA, Elbert ST, Gordon MS, Jensen JH, Koseki S, Matsunaga N, Nguyen KA, Su SJ, Windus TL, Dupuis M, Montgomery JA (1993) J Comput Chem 14:1347
- Frisch MJ, Trucks GW, Schlegel HB, Scuseria GE, Robb MA, Cheeseman JR, Montgomery JJA, Vreven T, Kudin KN, Burant JC, Millam JM, Iyengar SS, Tomasi J, Barone V, Mennucci B, Cossi M, Scalmani G, Rega N, Petersson GA, Nakatsuji H, Hada M, Ehara M, Toyota K, Fukuda R, Hasegawa J, Ishida M, Nakajima T, Honda Y, Kitao O, Nakai H, Kelna M, Li X, Knox JE, Hratchian HP, Cross JB, Adamo C, Jaramillo J, Gomperts R, Stratmann RE, Yazyev O, Austin AJ, Cammi R, Pomelli C, Ochterski JW, Ayala PY, Morokuma K, Voth GA, Salvador P, Dannenberg JJ, Zakrzewski VG, Dapprich A, Daniels AD, Strain MC, Farkas O, Malick DK, Rabuck AD, Raghavachari K, Foresman JB, Ortiz JV, Cui Q, Babou AG, Clifford S, Cioslowski J, Stefanov BB, Liu G, Liashenko A, Piskorz P, Komaromi I, Martin RL, Fox DJ, Keith T, Ak-Laham MA, Peng CY, Nanayakkara A, Challacombe M, Gill PMW, Johnson B, Chen W, Wong MW, Gonzalez C, Pople JA (2004) Gaussian03; Gaussian, Inc., Wallingford
- Wickrama Arachchilage AP, Feyer V, Prince KC, Wang F (2011) Synchrotron sourced X-ray photoemission spectroscopy of dipeptide phenylalanylphenylalanine, to be submitted
- Cossi M, Barone V, Cammi R, Tomasi J (1996) Chem Phys Lett 255:327
- Ayers P (2006) Theor Chem Acc 115:370
- Hirshfeld FL (1977) Theor Chim Acta 44:129
- Chong DP, van Lenthe E, van Gisbergen S, Baerends EJ (2004) J Comput Chem 25:1030
- van Leeuwen R, Baerends EJ (1994) Phys Rev A 49:2421
- Baerends EJ, Autschbach J, Bérces A, Bo C, Boerrigter PM, Cavallo L, Chong DP, Deng L, Dickson RM, Ellis DE, van Faassen M, Fan L, Fischer TH, Guerra CF, van Gisbergen SJA, Groeneveld JA, Gritsenko OV, Grüning M, Harris FE, van den Hoek P, Jacobsen H, Jensen L, van Kessel G, Kootstra F, van Lenthe E, McCormack D, Michalak A, Osinga VP, Patchkovskii S, Philipsen PHT, Post D, Pye CC, Ravenek W, Ros P, Schipper PRT, Schreckenbach G, Snijders JG, Solà M, Swart M, Swerhone D, te Velde G, Vernooijs P, Versluis L, Visser O, Wang F, van Wezenbeek E, Wiesenekker G, Wolff SK, Woo TK, Yakovlev A, Ziegler T (2006) Theo Chem ADF 2006.01, SCM; Vrije Universiteit, Amsterdam
- Selvam L, Vasilyev V, Wang F (2009) J Phys Chem B 113:11496
- Ahemd M, Ganesan A, Wang F, Prince K, Feyer V, Plekan O (2011) Determination of X-ray photoelectron spectra of β -lactam: core and valence, to be submitted
- Noorizadeh S, Dardab M (2010) Chem Phys Lett 493:376
- Cederbaum LS (1975) J Phys B At Mol Phys 8:290
- Cederbaum LS, Domcke W (1977) Adv Chem Phys 36:205
- von Niessen W, Schirmer J, Cederbaum LS (1984) Comput Phys Rep 1:57
- Zakrzewski VG, von Niessen W (1993) J Comput Chem 14:13
- Zakrzewski VG, Ortiz JV (1995) Int J Quantum Chem 53:583
- Wang F, Downton M, Kidwani N (2005) J Theor Comp Chem 4:247

32. Ganesan A, Wang F (2009) *J Chem Phys* 131:044321
33. NIST Mass Spec Data Center, S.E. Stein, director, “Infrared Spectra” in NIST Chemistry WebBook, NIST Standard Reference Database Number 69. PJ Linstrom and WG Mallard (eds), National Institute of Standards and Technology, Gaithersburg MD, 20899, <http://www.webbook.nist.gov> (retrieved October 28, 2009)
34. Scott AP, Radom L (1996) *J Phys Chem* 100:16502
35. Huang Z, Yu W, Lin Z (2006) *J Mole Struc Theochem* 758:195
36. Zhang G, Musgrave CB (2007) *J Phys Chem A* 111:1554
37. Wang F, Pang W, Duffy P (2011) *Mol Sim* (in press)
38. Akai N, Kudoh S, Takayanagi M, Nakata M (2002) *Chem Phys Lett* 356:133
39. Wilson HW (1974) *Spectrochimica Acta A* 30:2141
40. Akai N, Kudoh S, Nakata M (2005) *J Photochem Photobiol A Chem* 169:47
41. Huang Z, Yu W, Lin Z (2006) *J Mol Struct THEOCHEM* 758:195
42. Selvam L, Chen F, Wang F (2010) *Chem Phys Lett* 500:327
43. Jalkanen KJ, Degtyarenko IM, Nieminen RM, Cao X, Nafie LA, Zhu F, Barron LD (2008) *Theor Chem Acc* 119:191
44. Gristenko OV, van Leeuwen R, Baerends EJ (1995) *Phys Rev A* 52:1870
45. Wang F (2005) *J Mol Struct THEOCHEM* 728:31
46. Clark DT, Kilcast D, Adams DB, Musgrave WKR (1975) *J Electron Spectrosc Rel Phenom* 6:117
47. Xie Y, Sherwood MA (1991) *Chem Mater* 3:164
48. Fukui K, Yonezawa T, Shingu H (1952) *J Chem Phys* 20:722
49. Stener M, Fronzoni G, Decleva P (2005) *J Chem Phys* 122:234301
50. Fujisawa S, Ohno K, Masuda S, Harada Y (1986) *J Am Chem Soc* 108:6505
51. Ballard RE, Jones J, Sutherland E, Read D, Inchley A (1986) *Chem Phys Lett* 126:311
52. Duffot D, Flament JP, Heinesch J, Hubin-Franskin MJ (2000) *J Electron Spectrosc Relat Phenom* 113:79
53. Cradock S, Muir JM, Rankin DWH (1990) *J Mol Struct* 220:205
54. Onda M, Ohashi O, Yamaguchi I (1976) *J Mol Struct* 31:203
55. Spinrad B (1946) *J Am Chem Soc* 68:617
56. Caminati W, Melandri S, Favero LB (1994) *J Chem Phys* 100:8569
57. McQuidae BH, Banna MS (1988) *Can J Chem* 66:1919
58. Naves De Brito A, Svensson S, Keane MP, Karlsson L, Ågren H, Correia N (1992) *Europhys Lett* 20:205